PROGRESS IN COLOR, COLORANTS AND COATINGS

available online @ www.pccc.icrc.ac.ir

Ministry of Science, Research and Technology
Institute for Color Science and Technology

Progress in Color Colorants Coating 15 (2022), 355-366

Solution Combustion Synthesis of $MnAl_2O_4$ Brown Pigments Using Different Fuel Mixtures

A. M. Arabi*[1], Sh. Jebeli Moeen[2]

[1.] Department of Inorganic Pigments and Glazes, Institute for Color Science and Technology, P.O. Box: 16765-654, Tehran, Iran.

[2.] Central Lab, Institute for Color Science and Technology, P.O. Box: 16765-654, Tehran, Iran.

ARTICLE INFO

Article history:
Received: 01 Jan 2022
Final Revised: 22 Apr 2022
Accepted: 24 Apr 2022
Available online: 02 Jul 2022

Keywords:
Solution combustion synthesis
Ceramic pigment
$MnAl_2O_4$
Brown

ABSTRACT

This paper reports the synthesis of spinel manganese aluminates ($MnAl_2O_4$) brown pigments via microwave-assisted solution combustion using different urea-glycine fuel mixtures. The synthesized samples were analyzed through all the following methods: thermal analysis, X-ray diffractometry (XRD), scanning electron microscopy (SEM), and colorimetry. The results showed that amorphous flakes are obtained via one-step solution combustion under microwave radiation. They are then converted to the $MnAl_2O_4$ and minor structural changes due to manganese valence variation after calcination at 1000 °C. The mean crystallite size in the case of the fuel mixture after calcination at 1000 °C was 23 nm. The fuel type slightly affected the combusted flake-like microstructure before calcination. However, the porous flakes converted to nonporous nanoparticles after calcination by increasing the glycine content. The sample obtained by the combustion of fuel mixture (75:25 weight ratio) after calcination at 1000 °C had the highest reflection intensity, especially in the red region due to the formation of the $MnAl_2O_4$ crystal structure. The hue and saturation of the sample were 62.7 and 27.69, respectively. The red, yellow, and brightness coordinates were 12.69 (a), 24.61 (b*), and 45.76 (L*), respectively. As a result, the synthesized pigment can be a promising candidate for the production of ceramic inks compared with the commercial brown pigments [9.02 (a*), 13.62 (b*), and 33.61 (L*)]. The bandgap of the samples immediately after combustion was in the range of 4 eV, which was in good agreement with the results reported for the $MnAl_2O_4$ band gap (4.03 eV). Prog. Color Colorants Coat. 15 (2022), 355-366© Institute for Color Science and Technology.*

1. Introduction

Solution combustion synthesis (SCS), as a unique method, has found a special place in the synthesis of advanced materials such as catalysts, phosphors, pigments, etc. The essential advantages of SCS include simplicity, high reaction rate, high degree of porosity, and in-situ crystallization [1-3]. They have the properties such as electrocatalytic efficiency and ion selectivity. These properties have recently expanded to new fields, such as electrocatalysts [4] or corrosion inhibition [5].

*Corresponding author: aarabi@icrc.ac.ir

Recent efforts have used SCS along with other creative methods such as electrophoresis. Special nanocomposites such as zinc oxide/zinc sulfide (ZnO/ZnS) [6, 7], cadmium selenide/carbon nanotube (CdSe/CNTs) [8], and cadmium telluride/zinc sulfide (CdTe/ZnS) [9] were synthesized, which now have wide applications in biomedical. Undoubtedly, one of the most important categories of materials synthesized in this way are pigments [10, 11]. Different structures of pigments such as spinel, hexagonal, and perovskite have been synthesized. One of the most important pigments synthesized in the hexagonal structure is zinc oxide lonely [12] or with different dopants such as cobalt, iron, and copper [13, 14]. Also, in the perovskite structure, lanthanum aluminum oxide doped with chromium ($LaAlO_3$:Cr) red pigment can be mentioned [15]. Since spinel structures are organic pigments that hold large volumes of color centers as their unit of volume [16], the spinel is one of the most important structures synthesized by this method. Famous pigments such as deep blue cobalt aluminate ($CoAl_2O_4$) have been prepared by the SCS method [10, 17, 18].

Different parameters such as the type of organic fuel, oxidizing to fuel ratio, type of heating, pH value, etc., have been studied to achieve high-quality nano-powders [19-23]. The problem of obtaining a pigment with high dyeing value with a one-step combustion stage has been mentioned. For example, Shafiee chafi et al. [24] reported chromium doping in alumina and the formation of deep pink color with no need for a calcination step.

Among the items that significantly impact the combustion product is the type of heating using a heater, furnace, or microwave. Recently, researchers have been considered the use of microwaves in the field of combustion synthesis due to the more uniform heating of the precursors. Due to the high heating rate with these waves, the resulting microstructures are spongy, porous, semi-sintered forms filled with ultra-fine particles [13, 19-22].

The fine particle (submicron to nanoparticles) with a suitable crystallinity and deep color has suggested the pigments obtained by the combustion process as the right candidate for ceramic inks and toners [25-27]. The main property of the pigments used in the printing industry is the dispersibility in a variety of non-aqueous or aqueous media that arises from the fineness of the particles. Although the spinel pigments such as blue cobalt aluminate have been used in ceramic inks, the inks in the field of beige to brown color have limitations that spinel structures are still considered suitable candidates in this field.

Manganese oxide compounds have been used to make red to black pigments [28]. Manganese compounds such as MnO_2 have been used to develop the dark spinel pigments from black ($MnFe_2O_4$) to brown ($ZnMn_2O_4$) colors [29, 30]. Due to the development of the color in the presence of manganese in the range of brown to black, the use of strong spinel structures such as aluminate structures can contribute to structural and color stability. The aluminate host, which can be doped with different elements such as Cr, Mn, Fe, Co, Ni, shows the +a and +b region (quadrant-hot color) of the colorimetric diagram [30]. One of the pigments in this category, especially in the brown region, is manganese aluminate ($MnAl_2O_4$). Although some reports have been focused on the synthesis of wire-like particles of $MnAl_2O_4$ by doping the structure with Fe [31] or Pechini synthesis of $MnAl_2O_4$ for photocatalytic applications [32], less attention has been afforded to synthesizing $MnAl_2O_4$ as a brown ceramic pigment. In this study, the synthesis of $MnAl_2O_4$ as a ceramic pigment has been investigated. The effect of the important parameter of the fuel mixture has been carefully evaluated.

2. Experimental

All the chemicals were of analytical grade and purchased from Merck Co. (Germany). The oxidizers were manganese nitrate hexahydrate ($Mn(NO_3)_2.6H_2O$) and aluminum nitrate nonahydrate ($Al(NO_3)_3.9H_2O$). The fuels were glycine and urea. The combustion reactions were balanced separately for each fuel based on propellant chemistry. In this method, the capacity of nitrogen is assumed to be zero because it does not participate in reduction and oxidation reactions. The balanced reactions for glycine and urea are as follows (Eqs. 1 and 2):

$$Mn(NO_3)_2.6H_2O + 2Al(NO_3)_3.9H_2O + \frac{40}{6} CH_4N_2O \text{ (glycine)} \rightarrow MnAl_2O_4 + \frac{40}{6}CO_2 + \left(\frac{80}{6} + 15\right) H_2O + \frac{152}{12} N_2 \quad (1)$$

$$Mn(NO_3)_2.6H_2O + 2Al(NO_3)_3.9H_2O + \frac{40}{9} C_2H_5NO_2 \text{ (urea)} \rightarrow MnAl_2O_4 + \left(\frac{80}{9} + 15\right) CO_2 + \frac{100}{9} H_2O + \frac{112}{18} N_2 \quad (2)$$

Several fuel mixtures containing 0, 25, 75, and 100 weight ratios for each fuel were used, for example, 0.52 g $Mn(NO_3)_2.6H_2O$ and 2.17 g $Al(NO_3)_3.9H_2O$ were dissolved in 20 mL deionized water to obtain 0.5 g $MnAl_2O_4$ in the case of glycine fuel according to Eq. 1. After thorough dissolution, 1.45 g glycine was added under stirring. Meanwhile, the temperature gradually increased to 80 ºC to obtain a viscous gel after 30 min. The gel was transferred to the microwave oven (Samsung) to conduct the combustion reaction at 900 watts for 3 minutes. The reaction occurred rapidly with massive fume, as shown schematically in Figure 1. The reaction product is usually dark due to the high combustion reaction rate and insufficient oxygen in the reaction medium. So, the as-synthesized powder was calcined at 500 and 1000 ºC to obtain the desired brown pigment.

In the case of urea fuel, 0.52 g $Mn(NO_3)_2.6H_2O$, 2.17 g $Al(NO_3)_3.9H_2O$ and 0.77 g urea were used to obtain 0.5 g $MnAl_2O_4$ pigment according to Eq. 2. A variety of weight ratios of glycine to urea (25, 50, and 75) were prepared using the above-calculated amounts of fuel (i.e.,1.45 g glycine and 0.77 g urea) to investigate the effect of the fuel mixture. So, the fuel mixture with the ratio of 75:25 (U25G75) had 1.09 g glycine and 0.19 g urea. Similarly, the fuel mixtures with the glycine to urea weight ratios of 25:75 and 50:50 were designated as U75G25 and U50G50, respectively. After calcination at 500 and 1000 ºC, the samples were labeled as U25G75-500, U50G50-500, U75G25-500, and U25G75-1000, U50G50-1000, U75G25-1000, respectively.

The samples were characterized using an X-ray diffractometer (XRD, Siemens D500) and a scanning electron microscope (SEM, 1455 VP UK). The reflection spectrum and CIELAB color coordinates (C* and L based on L*, a*, and b*) were analyzed using a spectrophotometer (7000A Gretag MacBeth). The thermal behavior of the calcined samples was investigated by simultaneous thermal analysis (STA, PL-STA-1640).

3. Results and Discussion

3.1. Structural studies

Figure 2 shows XRD patterns of $MnAl_2O_4$ pigments synthesized with different fuel mixtures before calcination (i.e., U25G75, U75G25, and U50G50). It could be seen that these particles were amorphous with some weak peaks at 2θ=30°, the intensity of which is relatively higher for the U25G75 sample. In other words, the fuel mixture may also affect the disorderly amorphous nature of the synthesized samples even before calcination.

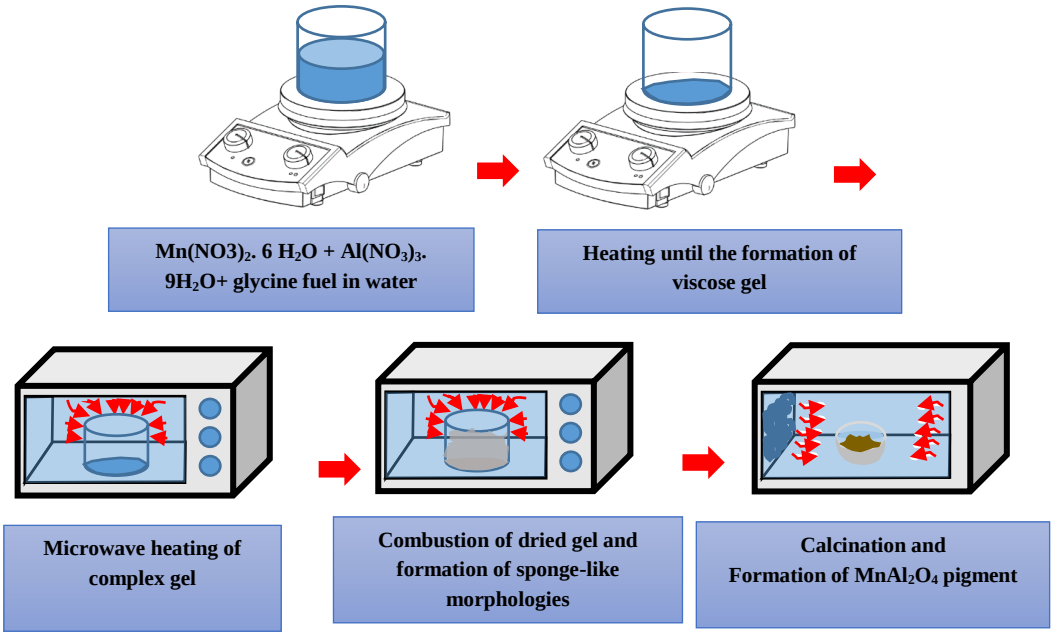

Figure 1: Sample preparation steps.

As shown by XRD patterns in Figure 3 for U25G75-1000, U50G50-1000, U75G25-1000 samples, calcination at 1000 ºC led to the combination of different crystalline Manganese Aluminum Oxide phases (JCPDS Numbers: 00-001-1302, 00-010-0310, 00-029-0880, 00-029-0881) with cubic structure, Fd3m space group, lattice parameter about 8.2 Å. Navarro et al. [33] was also reported that 1000 ºC calcination is a suitable temperature for the purification of $MnAl_2O_4$ structure. However, different phases of Manganese Aluminum Oxide developed because the pure phase of $MnAl_2O_4$ spinel requires heat treatment in the temperature range of 1000 to 2000 °C and in special atmospheric conditions.

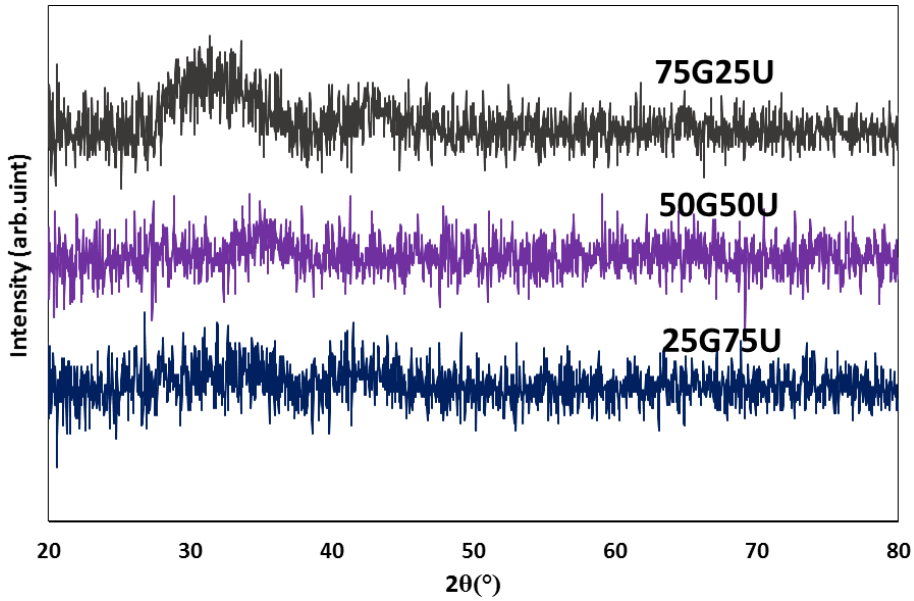

Figure 2: XRD patterns of $MnAl_2O_4$ pigments synthesized using different weight ratios of urea to glycine before calcination.

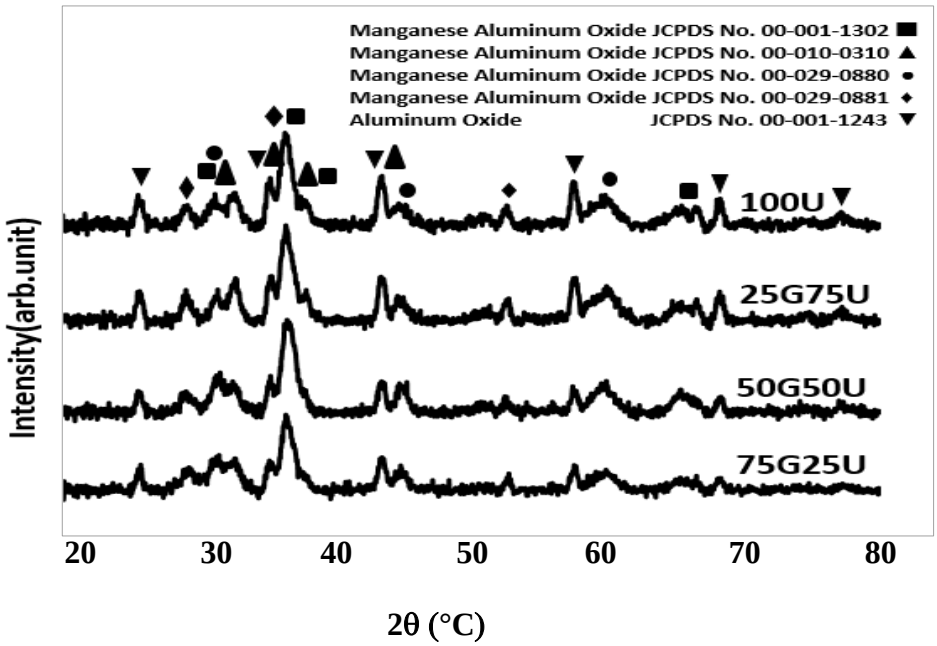

Figure 3: XRD patterns of $MnAl_2O_4$ pigments synthesized using different weight ratios of urea to glycine after calcination at 1000 ºC.

Manganese has multiple capacities of +2, +3, and +4, while the capacity of two is in stable conditions. Therefore, calcination temperature and atmospheric conditions are essential to achieve a stable structure, which is not very controllable in the combustion method [33]. The mean crystallite size calculated based on the Scherrer equation [34] was 23 nm, confirming the capability of the combustion method in producing nano-crystallite powders. In other words, the nano-crystallites were so fine that the thermal driving force at 1000 ºC has not been able to change their size. On the other hand, the phase purity increased by increasing the glycine content, indicating that the fuel type significantly influences the crystallinity.

3.2. Thermal analysis

Figure 4 shows the TG/DTA/DTG curve of the metal nitrates, and CH_4N_2O (glycine fuel) complex. There are five weight losses: (i) physical water removal, (ii) dehydration, (iii) combustion reaction, (iv) oxidation of residual organic compounds, and (v) removal of residual nitrate.

A weight loss with a weak endothermic peak (peak 1) occurred from room temperature to 90 °C due to the physical water evaporation. In the second step, the mixture of glycine and metal nitrates was dehydrated with an endothermic peak (peak 2) between 80 and 120 °C The next and the main step was the combustion reaction, which occurred in a wide range between 120 and 320 °C with a maximum exothermic DTA peak at 260 °C (peak 3). The NO^{3-} ions and the glycine compound react enclosed in the gel structure at this stage. Also, H_2O, CO_2, and N_2 exhaust gases are removed from the system. The remaining organic matter from the combustion process was burned in the fourth step. This process was associated with the combustion process, and therefore no separate exothermic peak was observed. In the final stage, excess unreacted nitrate ions were also removed from the system. However, the second exothermic peak (peak 4) can be seen at 480 to 780 °C, accompanied by a slight mass loss. As a result, this peak can be related to the crystallization process. According to the TG/DTA curves, the minimum temperature required to remove impurities and the formation of a crystallized phase was 800 °C [8]. Tang et al. [35] showed that the glycine burning process occurs at 200 to 400 °C and is exothermic in two parts. They also showed that the above 400 °C exothermic peak is related to the crystallization of the oxide structure. The inset shows the TG/DTA/DTG curves of the as-synthesized powder. The reaction proceeded well in the combustion of the gel, and the as-synthesized powder showed only a reduction in weight due to the residual volatiles, and as a result, no intense exothermic or endothermic peaks were observed in the DTA curve.

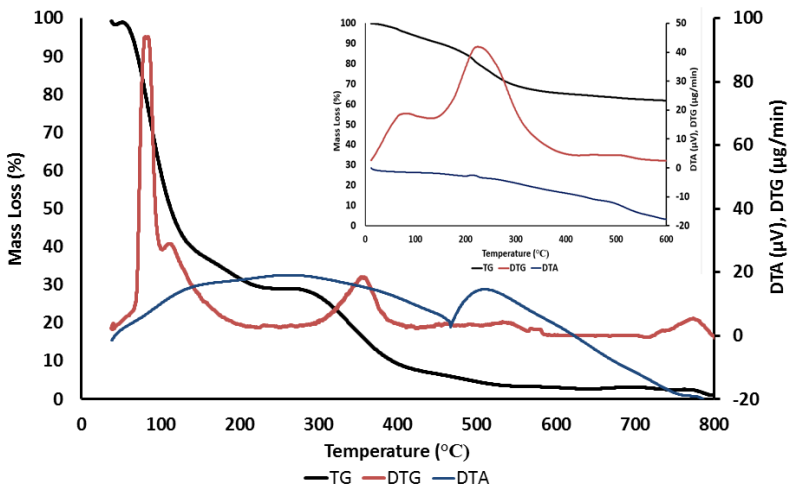

Figure 4: TG/DTA/DTG curves of metal nitrates and CH_4N_2O (glycine fuel) complex mixture (The inset shows the TG/DTA/DTG curves of the as-synthesized powder).

3.3. Morphological studies

SEM images of U25G75, U75G25, and U50G50 samples are shown in Figure 5. It can be seen that all the samples had amorphous and non-particulate morphology. The thick gel has been converted to thin flakes under microwave exposure and then became porous due to the emission of gases like CO_2, H_2O, and N_2 upon combustion of organic fuels. The obtained amorphous product was brittle and did not need further milling, specifically in the case of urea and glycine fuels that contained amine groups. These groups have two explicit effects: (i) increasing the combustion reaction rate and (ii) decomposition of part of fuel-metal nitrate before combustion, which ignites in the subsequent stages [23]. In other words, glycine is a zwitterion, which can be complex with both its carboxylic acid group and its amino acid group with metal ions. The Xerogel (Dried powder product from complex nitrate-fuel gel) is decomposed into carbon-nitrogen, metal-nitrogen bonds, and amino acid groups during the dehydration and heating process. In the next step, a series of multiple decompositions eventually leads to the decomposition of nitrate and the beginning of the combustion process. The initial decomposition of fuel into amine groups before combustion acts as a firecracker, resulting in more homogenous porous microstructures [36, 37]. The comparison of samples revealed that the flakes become finer by increasing the glycine content mainly due to the higher combustion heat, higher combustion rate, and higher momentum in this fuel.

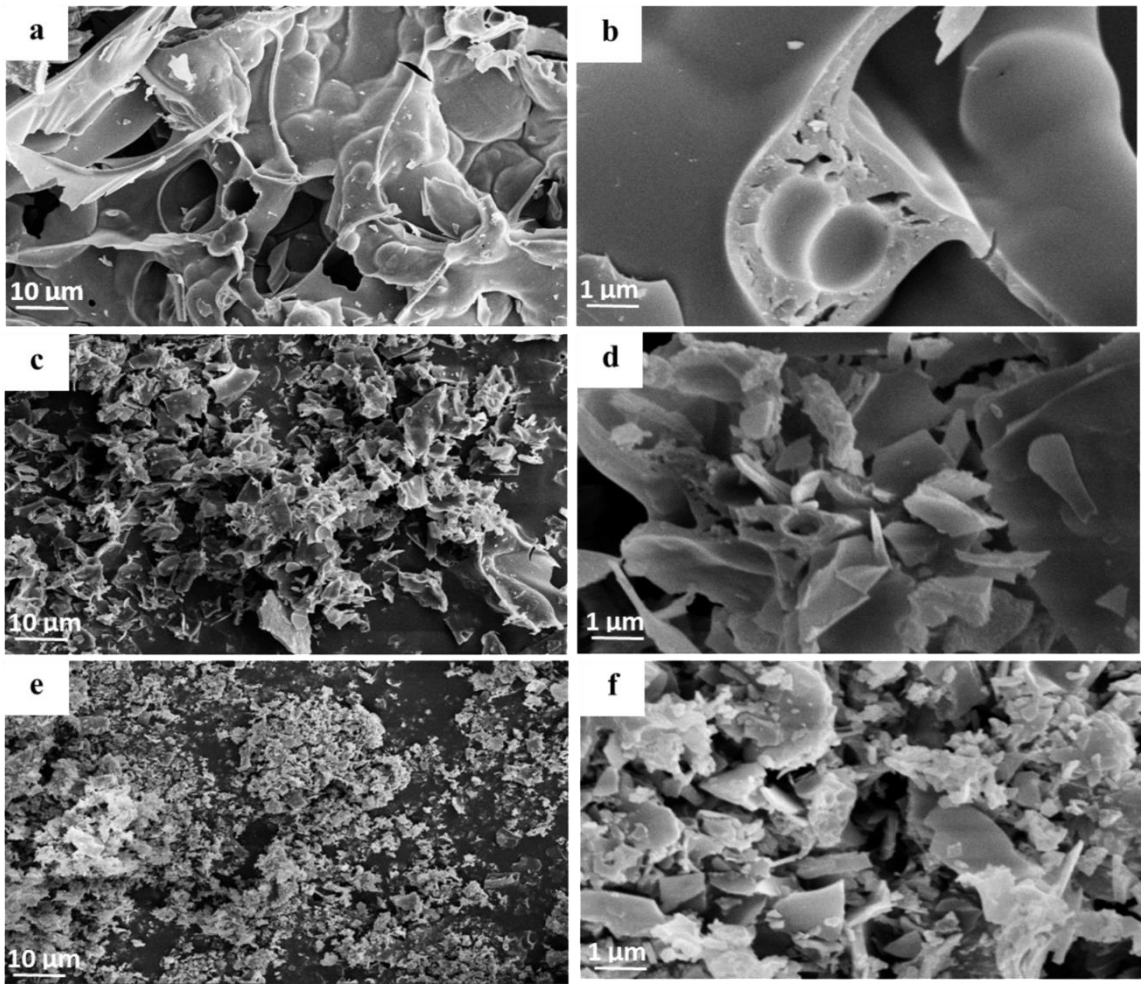

Figure 5: SEM images of $MnAl_2O_4$ pigments synthesized using different weight ratios of urea to glycine before calcination: (a, b) U75G25, (c, d) U50G50, and (e, f) U25G75.

Figures 6 and 7 show SEM images of samples calcined at 500 and 1000 °C. Deformation of the flakes was indicative of incomplete combustion and the emission of carbon before calcination. In addition, the flakes became coarser upon calcination at 500 °C. It is worth noting that nanoparticles could be observed on the surface of flakes after calcination at 1000 °C. The combustion front mainly was concentrated on the surface of the flakes, which is in good agreement with the structure formation mechanism; the structure is amorphous at room temperature and crystallizes by increasing the temperature. In other words, there is a high correlation between structure and microstructure. It is evident from SEM images that nanoparticles are not even detectable in samples calcined at 500 °C, but they begin to grow by increasing the temperature. It can be inferred that the combustion reaction rate is so high that the nanoparticles need to be heated to 1000 °C to become visible, which can be considered an advantage of the combustion method that nanoparticles remain below 100 nm even after heating to 1000 °C. Despite this, the fuel type has a considerable effect on the temperature of nanoparticle formation. In addition, U25G75-1000 has been identified as the sample with the most microstructural conversion. It could convert from flake-like to nanoparticulate morphology among all the samples.

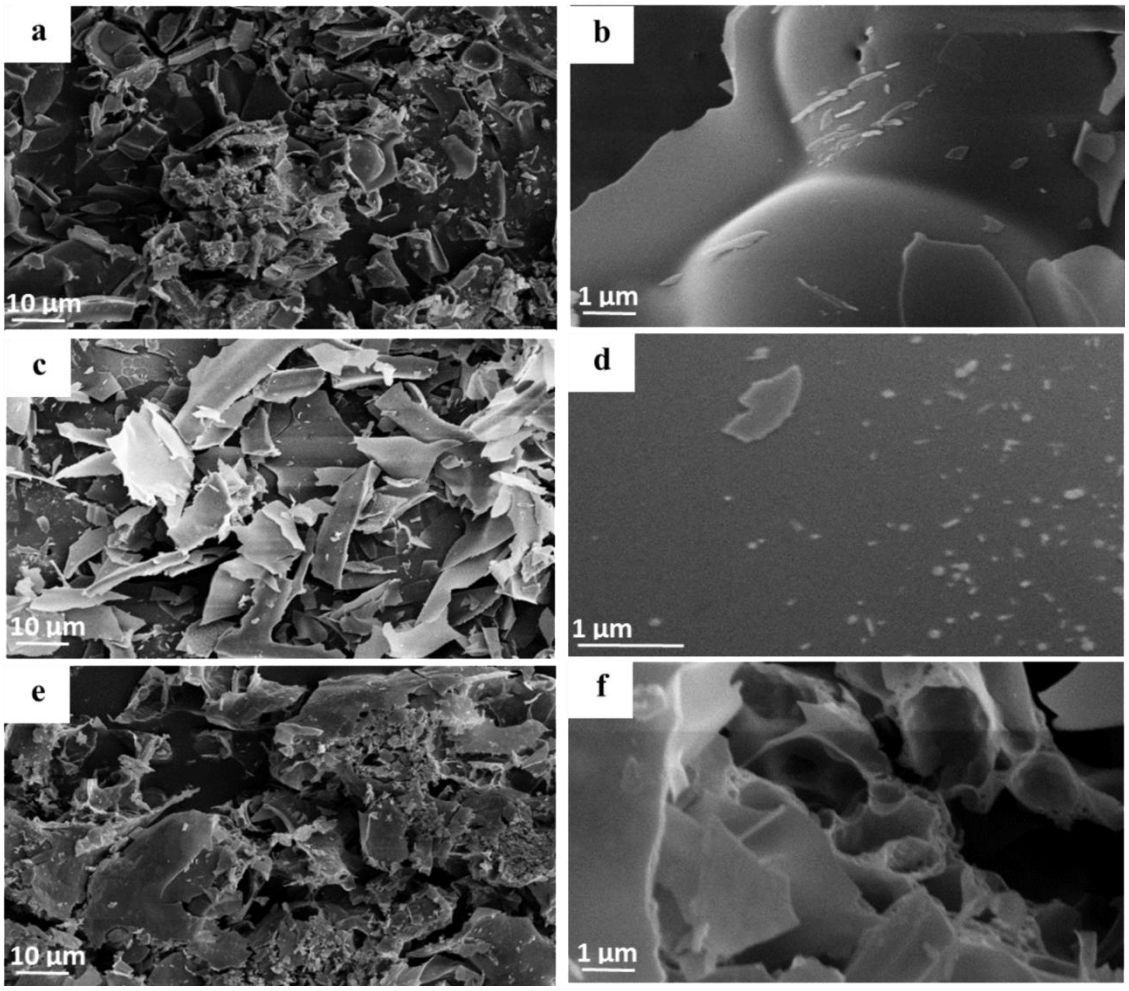

Figure 6: SEM images of $MnAl_2O_4$ pigments synthesized using different weight ratios of urea to glycine after calcination at 500 ˚C: (a,b) U75G25, (c,d) U50G50, and (e,f) U25G75.

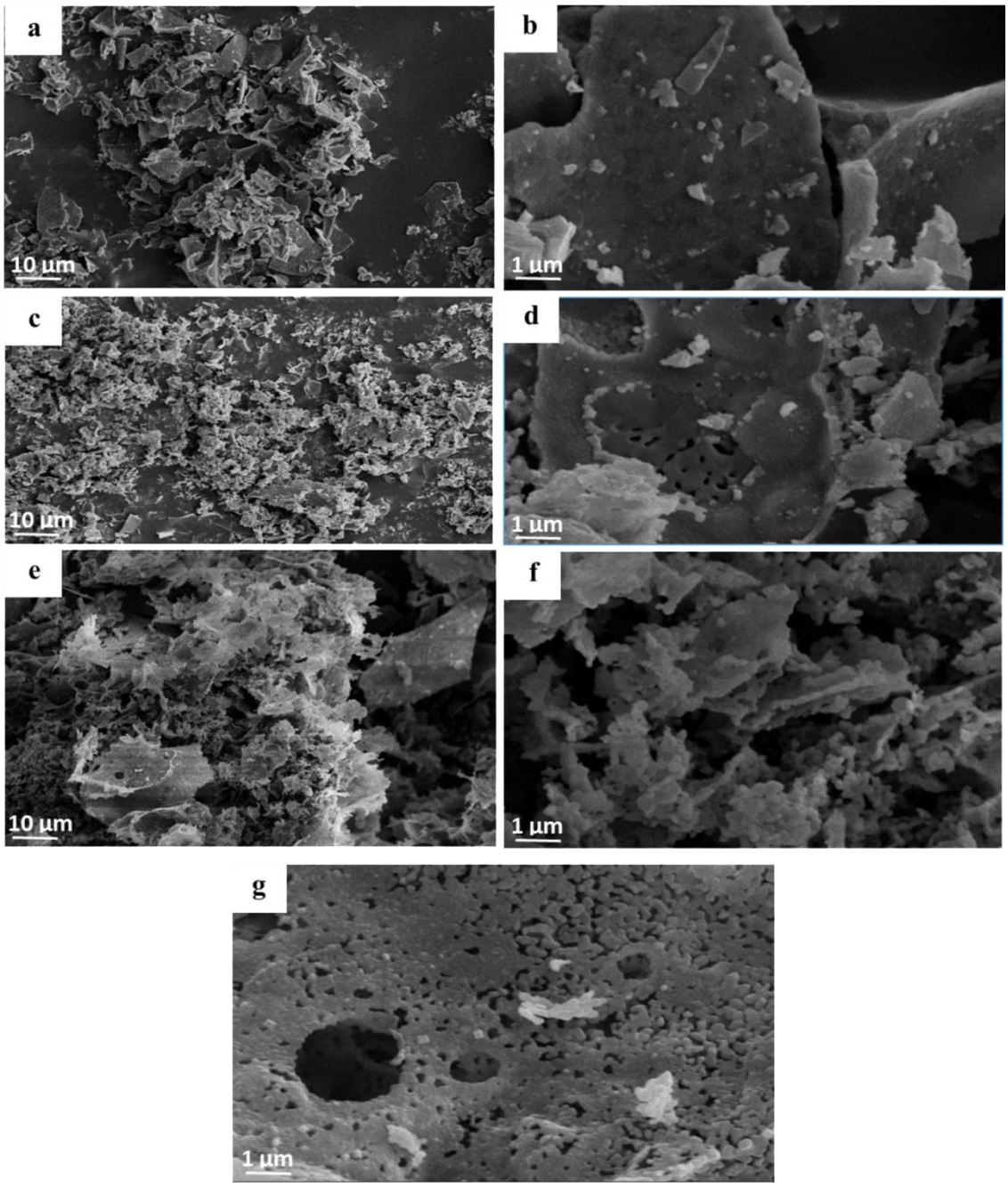

Figure 7: SEM images of $MnAl_2O_4$ pigments synthesized using different weight ratios of urea to glycine after calcination at 1000 ºC: (a,b) U100, (c, d) U75G25, (e, f) U50G50, and (g) U25G75.

3.4. Colorimetry and optical properties

The color characteristics of the synthesized samples using different weight ratios of urea and glycine are presented in Table 1. It could be seen that although most of the pigments had dark color before calcination, they turned to brown color after heat treatment. The positive effect of heat treatment on obtaining the desired color was proven by the increase in the value of both hue (h) and saturation (C*).

After calcination at 1000 ºC, surface carbon layers were removed, resulting in higher lightness (L) values. Increasing the glycine content resulted in an increase in hue from 52.6 to 62.7, and the saturation also rose from 15 to 27.69. So, U25G75-1000 can be considered the optimum sample. This behavior was different for fuel mixtures without glycine. For example, U-1000 was in second place in C* and h values. An example of a commercial brown pigment has 9.02, 13.62, and 33.61 a^*, b^*, and L^* values, respectively [38]. So the U25G75-

1000 sample can be introduced as a suitable brown pigment.

The variation of reflectance also follows the same trend. According to Figure 8, U25G75-1000 was the optimum sample. However, by further decreasing the glycine content below 25 %, no significant variations were observed in the reflectance. The reflectance spectra of samples calcined at 500 °C indicated that this temperature has not been appropriate for obtaining the desired brown pigment. During calcination, carbon was removed from these samples, increasing the reflectance.

The brown color can also be assessed in red (a*) and yellow (b*) coordinates. A simultaneous increase in a* from 9.1 to 12.6 and b* from 11.9 to 24.6 was observed by increasing the glycine content. In the case of the U25G75-1000 sample, these values increased from 3.5 to 12.6 and from 5.27 to 24.6, respectively. This sample's h and C* values increased to above 60 and 27, respectively. All these parameters were increased somewhat linearly by increasing the glycine content in the fuel mixture. It also seems possible to predict the color of a mixture by calibrating these parameters and establishing a correlation between structure, microstructure, and color variations.

Table 1: Color characteristics of $MnAl_2O_4$ pigments synthesized using different weight ratios of urea to glycine.

Sample	a*	b*	L*	C*	h	Calcination temperature (°C)	Glycine content (wt%)	Urea content (wt%)
U25G75-1000	12.69	24.61	45.76	27.69	62.72	1000	75	25
U50G50-1000	9.53	16.22	42.34	18.82	59.57	1000	50	50
U75G25-1000	10.02	12.63	32.47	16.12	51.57	1000	25	75
U75G25-500	2.06	2.36	26.32	3.14	48.87	500	25	75
U25G75-500	3.52	5.27	32.43	6.34	56.25	500	75	25
U50G50-500	3.09	3.95	28.29	5.02	51.95	500	50	50
U25G75-500	3.82	5.84	33.16	6.98	56.86	500	75	25
U25G75	2.25	2.98	27.57	3.73	52.94	-	75	25

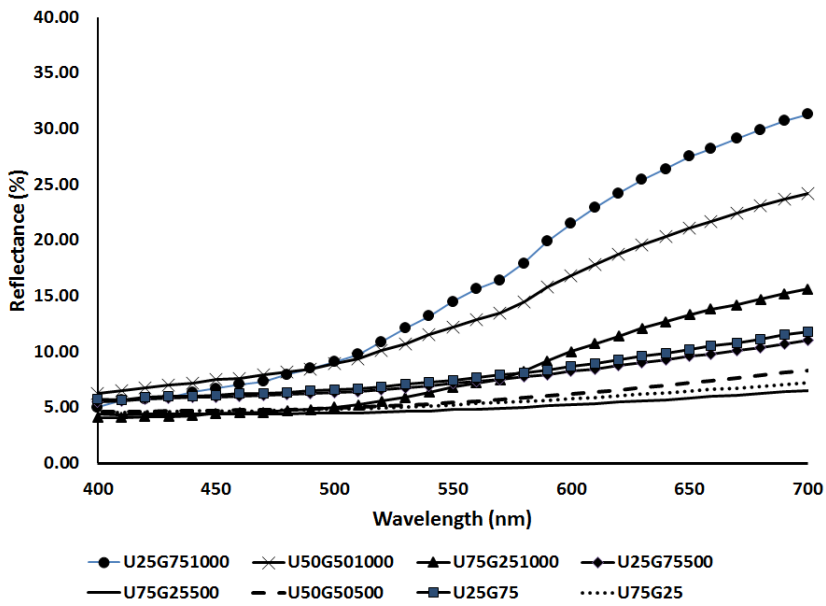

Figure 8: Reflectance spectra of $MnAl_2O_4$ pigments synthesized using different weight ratios of urea to glycine.

The CIE diagram shown in Figure 9 was utilized to investigate the color characteristics of the optimum sample. As a result, the U25G75-1000 sample showed the purest brown color, which was evident from the photographs presented.

Figure 10 shows the method to calculate the band gap values (E_g) of the samples synthesized in the presence of urea, glycine, and urea-glycine fuel mixture (U50G50 sample). The curves were plotted using the reflection spectra and the kubelka-Munk equation. The kubelka-Munk values were calculated using equation 3.

$$F(R) = \frac{(1-R)^2}{2R} \quad (3)$$

F (R) is the Kubelka-Munk function, and R is the reflective fraction. To estimate the bandgap, $[F(R)h\nu]^2$ was plotted in terms of hν. hν is the unit of energy in terms of eV. The x-intercept value is the determined value of E_g. The estimated values of Eg for the samples were in the range of 4 eV, which is consistent with the estimated values for the $MnAl_2O_4$ nanoparticles [39]. As can be seen, the sample obtained in the presence of the fuel mixture has a narrower bandgap and is closer to the visible range. The mixed state of fuels is composed of more structural defects, and the band between the band gap has been significantly reduced. Another reason for the decrease of the bandgap is the favorable conditions for the formation of nanoparticles in the mixed fuel state. The nanoparticles are observed in the porous sponge walls after combustion and calcination only in mixed fuel conditions. The matrix (spongy, porous structure) has a wider bandgap, and the nanoparticles formed to make the bandgap narrower and closer to the visible range [40].

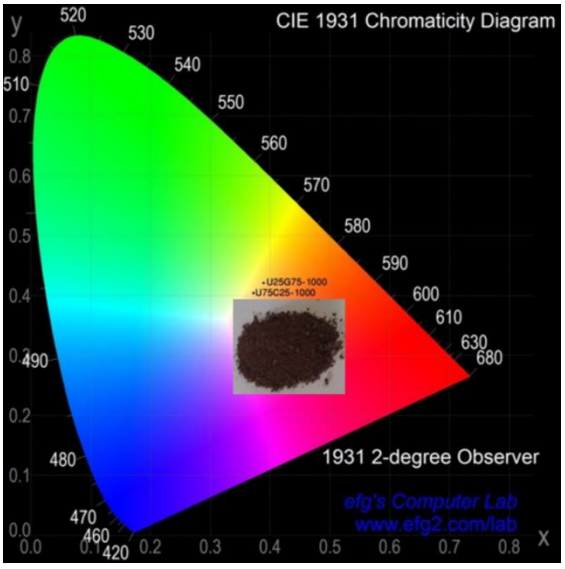

Figure 9: CIE diagram of the optimum $MnAl_2O_4$ pigments (U25G75-1000 and U75C25-1000). The inset shows the photograph of $MnAl_2O_4$ brown pigment (U25G75-1000).

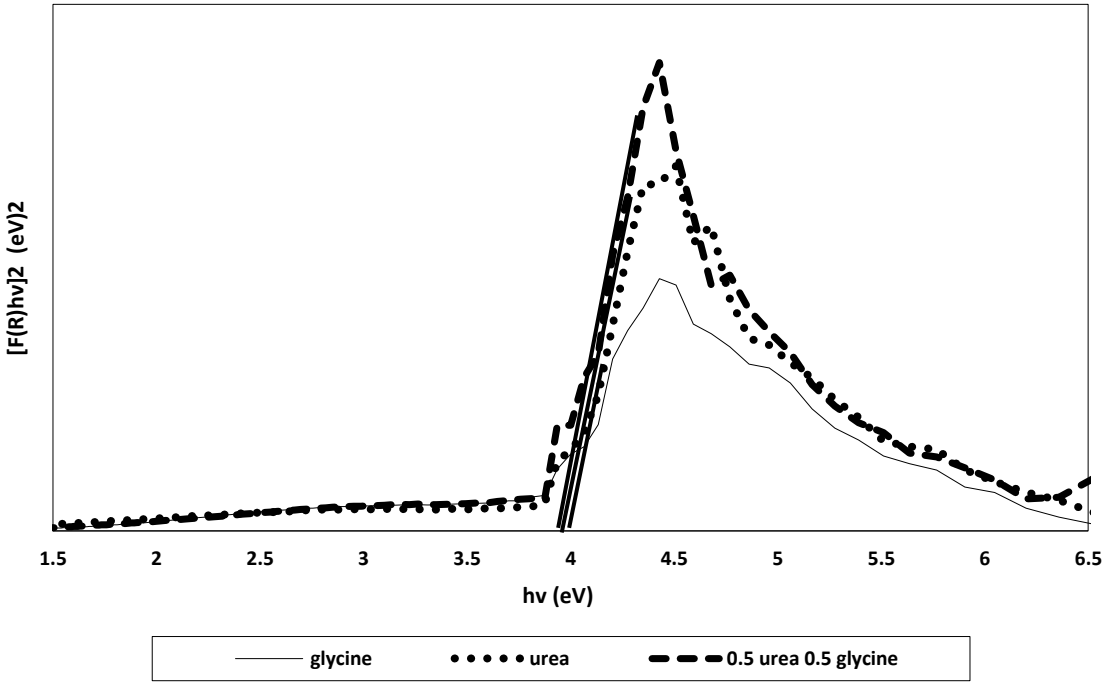

Figure 10: The plot of $[F(R)h\nu]^2$ versus hν to determine the band gap of samples synthesized in the presence of glycine, urea and U50G50 fuel mixture.

4. Conclusion

In this work, $MnAl_2O_4$ brown pigments were synthesized via the solution combustion method. Thermal analysis revealed two endothermic peaks due to water evaporation and gelation. Also, It was shown two exothermic peaks related to the combustion and phase transformation of the aluminate product. XRD results showed that the aluminate phase could not be achieved directly through one-step combustion synthesis. Rather, a hydroxide compound is formed as an intermediate product converted to single-phase aluminate by heating at 1000 ˚C. SEM images indicated that the fuel type significantly affects the combustion, hence the final microstructure. It can be suggested that the combustion process may initiate from the surface of the flakes formed during the gelation step, and then nanoparticles are crystallized by increasing the temperature. The complete conversion of porous flakes to nanoparticles occurred in the U25G75 sample. The best color characteristics were obtained for U25G75 sample (h=62.7, C*=27.69, a*=12.69, b*=24.61, and L*=45.76). As a result, it can be concluded from the results that the combination of combustion synthesis and heat treatment, especially in the presence of fuel mixtures, may result in brown nano pigments appropriate for ceramic inks.

5. References

1. A. Varma, A. S. Mukasyan, A. S. Rogachev, K. V. Manukyan, Solution Combustion Synthesis of Nanoscale Materials, *Chem. Rev.*, 116(2016), 14493-14586.
2. F. Deganelloa, A. Kumar Tyagi, Solution combustion synthesis, energy and environment: Best parameters for better materials, *Prog. Cryst. Growth Charact. Mater.*, 64 (2018), 23-61.
3. E. Novitskaya, J. P. Kelly, S. Bhaduri, O. A. Graeve, A review of solution combustion synthesis: an analysis of parameter controlling powder characteristics, *Int. Mater. Rev.*, 66(2021), 188-214.
4. Z. Yavari, Z. Ghahramani, A. M. Arabi, M. Noroozifar, Nanosized palladium loaded on porous ceria: A three-dimensional boosted electrocatalyst for electrooxidation of C1 compounds, *Int. J. Hydrogen. Energy*, 45(2020), 21319-21330.
5. Z. Ghahramani, A. M. Arabi, M. Shafiee Afarani, M. Mahdavian, Solution combustion synthesis of cerium oxide nanoparticles as corrosion inhibitor, *Int. J. Appl. Ceram. Technol*., 17(2020), 1514-1521.
6. M. Zahiri, M. Shafiee Afarani, A. M. Arabi, Dual functions of thiourea for solution combustion synthesis of ZnO/ZnS composite powders: fuel and sulphur source, *Appl. Phys. A.*, 124(2018), 1-6.
7. M. Zahiri, M. Shafiee Afarani, A. M. Arabi, Combustion synthesis of ZnO/ZnS nanocomposite phosphors, *J. Fluoresc.*, 29 (2019), 1227-1239.
8. B. Karimi, A. M. Arabi, F. Najafi, M. Shafiee Afarani, CNT–CdSe QDs nanocomposites: synthesis and photoluminescence studies, *J. Mater. Sci. Mater.*, 29 (2018), 13499-13507.
9. H. Shirzadeh Derabi, M. Shafiee Afarani, A. M. Arabi, D. Mohebbi Kalhori, Co-precipitation Synthesis of CdTe/ZnS, ZnSe, CdS and CdSe Core-Shell Quantum Dots, *J. Color. Sci. Technol.*, 13(2019), 89-98.
10. T. Tatarchuk, A. Shyichuk, J. Lamkiewicz, J. Kowalik, Inversion degree, morphology and colorimetric parameters of cobalt aluminate nanopigments depending on reductant type in solution combustion synthesis, *Ceram. Int.*, 46(2020), 14674–14685.
11. S. Mestre, M.D. Palacios, P. Agut, Solution Combustion Synthesis of $(Co,Fe)Cr_2O_4$ pigments, *J. Eur. Ceram. Soc.*, 32(2012), 1995-1999.
12. S. Rasouli, Sh. Saket. One Step Rapid Synthesis of Nano-Crystalline ZnO by Microwave-AssistedSolution Combustion Method, *Prog. Color Colorants Coat.*, 3(2010), 19-25.
13. S. Rasouli, M. Valefi, S. J. Moeen, A. M. Arabi, Microwave-assisted gel combustion synthesis of ZnO-Co nano-pigments, *J. Ceram. Process. Res.*, 12 (2011), 450-455.
14. X. Kang, C. Li, Z. Zheng, X. Cui, Synthesis of ZnO and Cu-doped ZnO nanocrystalline by solution combustion method and their catalytic effects on thermal behavior of $KClO_4$, *Combust. Sci. Technol.*, 193(2021), 75-89.
15. R. Ianoş, R. Lazău, R. Băbuţă, E. Muntean, E. A. Moacă, C. Păcurariu, Solution combustion synthesis: a straightforward route for the preparation of chromium-doped lanthanum aluminate, $L_aAl_{1-x}Cr_xO_3$, pink red pigments, *Dyes. Pigm.*, 155(2018), 218-224.
16. M. Dondi, M. Blosi. D. Gardini, Z. Chiara, Ceramic pigments for digital decoration inks: an overview, *Ceram. Forum Int.*, 89(2012), E59-E64.
17. Sh. Salem, S.H. Jazayeri, A. Allahverdi, M.Shirvani, $CoAl_2O_4$ Nano pigment obtained by combustion synthesis, *Int. J. Appl. Ceram. Technol.*, 9(2012), 968-978.

18. Sh. Salem, S.H. Jazayeri, F. Bondioli, A. Allahverdi, M. Shirvani, Synthesis conditions of cobalt aluminate nano-sized powder, *J. Ceram. Sci. Technol.*, 2(2011), 169-178.
19. S. Rasouli, A. M. Arabi, High speed preparation of $GdCaAl_3O_7$:Eu nano-phosphors by microwave-assisted combustion approach, *Prog. Color Colorants Coat.*, 3(2010), 110-117.
20. S. Rasouli, A. M. Arabi, A. Naeimi, S. M. Hashemi, Microwave-assisted combustion synthesis of ZnO:Eu nanoparticles: effect of fuel types, *J. Fluoresc.*, 28(2018), 167-172.
21. D. Bovand, A. M. Arabi, M. Bovand, Microwave assisted solution combustion synthesis of β-tricalcium phosphate nano-powders, *Bol. Soc. Esp. Ceram. Vidrio.*, 57(2018), 240-246.
22. M. Shahmirzaee, M. Shafiee Afarani, A. Iran Nejhad, A. M. Arabi, Microwave-assisted combustion synthesis of $ZnAl_2O4$ and ZnO nanostructure particles for photocatalytic wastewater treatment, *Part. Sci. Technol.*, 37 (2019), 110-117.
23. M. Zahiri, M. Shafiee Afarani, A. M. Arabi, Synthesis of zinc oxide and zinc oxide/zinc sulfide nano composite via solution combustion route, *Mater. Res. Express.*, 6(2019), 1250g5.
24. M. Shafiei Chafi, B. Ghasemi, A.M. Arabi, Solution combustion synthesis (SCS) of chrome alumina as a high temperature pink pigment, *Int. J. Appl. Ceram. Technol.*, 15(2018), 203-209.
25. M. Ataeefard, A. M. Aarabi, Producing ceramic toner via emulsion aggregation method based on $ZrSiO_4$: Pr ceramic pigment, *Prog. Color Colorants Coat.*, 14(2021), 113-120.
26. K. Mokhtari, Sh. Salem, A novel method for the clean synthesis of nanosized cobalt based blue pigments, *RSC. Adv.*, 7(2017), 29899-29908.
27. P. Xiaojin, Z. Qi, C. Jinshu, Y. Jian, W. Ya, J. Junnan, Preparation and characterization of a stable nano-$CoAl_2O_4$ ink for glass decoration by ink-jet printing, *Mater. Res.*, 20(2017), 1340-1344.
28. B. Tanisan, S. Turan, Synthesis of Fe-Mn black pigments by using hematite waste and manganese ore mixtures, *Trans. Indian .Ceram. Soc.*, 71(2012),17-20.
29. L. J. Almeida,E. C. Grzebielucka,S. R. M. Antunes, C. P. F. Borges, A. V. C. de Andrade,É. C. F. de Souza, Synthesis of brown inorganic pigments with spinel structure from the incorporation of spent alkaline batteries, *Mater. Res.*, 23(2020), e20190515.
30. D. F.L. Horsth, J. O. Primo, M. Dalpasquale, C. Bittencourt, F. J. Anaissi, Colored aluminates pigments obtained from metallic aluminum waste, an opportunity in the circular economy, *Clean. Eng. Technol.*, 5(2021), 100313.
31. A. Shafiekhani, H. Saeid Firozeh, Influence of Fe@$MnAl_2O_4$ and synthesis of novel compound $Mn_{0.83}Fe_{0.21}Al_{1.96}O_4$, *Phys. B: Condens. Matter.*, 421(2013) 122–126.
32. M. Edrissi, M. Soleymani, M. Naderi, Synthesis of $MnAl_2O_4$ nanocrystallites by Pechini and sequential homogenous precipitation methods: characterization, product comparison, photocatalytic effect, and Taguchi optimization, *J. Sol-Gel. Sci. Technol.*, 64(2012), 485-492.
33. R. C.S.Navarro, R. R.de Avillez, T. FreireGoes, A. M.S.Gomes, Low temperature thermal and volumetric behavior of $MnAl_2O_4$ spinel, *J. Mater. Res. Technol.*, 9(2020), 4194-4205.
34. A. L. Patterson, The scherrer formula for X-Ray particle size determination, *Phys. Rev.*, 56(1939), 978-982.
35. Y. Tong, J. Ma, S. Zhao, H. Huo, H. Zhang, A salt-assisted combustion method to prepare well-dispersed octahedral $MnCr_2O_4$ spinel nanocrystals, *J. Nanomater.*, 2015, 214978.
36. Sh. M. Khaliullin,V. D. Zhuravlev, V. G. Bamburov, A. Khort , S. I. Roslyakov, G. V. Trusov, D. O. Moskovskikh, Effect of the residual water content in gels on solution combustion synthesis temperature, *J. Sol-Gel Sci. Technol.*, 93(2020), 251–261.
37. L.A. Chick, L.R. Pederson, G.D. Maupin, J.L. Bates, L.E. Thomas and G. J. Exarhos, Glycine-nitrate combustion synthesis of oxide ceramic powders, *Mater. Lett.*, 10(1990), 6-12.
38. K. W. Bort, H.R. Ferreira,D. Galante, F. J. A. Marcia, G. P. Valenga, Structural and morphological behaviour and study of the colorimetric and reflective properties of commercial inorganic pigments, *S. Afr. J. Chem.*, 72(2019), 215-221.
39. P. Bhavani, A. Manikandan, S.K. Jaganathan, S. Shankar, S. A. Antony, Enhanced catalytic activity, facile synthesis and characterization studies of spinel Mn–Co aluminate nano-catalysts, *J. Nanosci. Nanotechnol.*, 18(2018), 1388-1395.
40. R. N. Abed, M. Kadhom,D. S. Ahmed,A. Hadawey, E. Yousif, Enhancing optical properties of modifed PVC and Cr_2O_3 nanocomposite, *Trans. Electr. Electron. Mater.*, 22(2021), 317-327.

How to cite this article:
A. M. Arabi, Sh. Jebeli Moeen, Solution Combustion Synthesis of $MnAl_2O_4$ Brown Pigments Using Different Fuel Mixtures. Prog. Color Colorants Coat., 15 (2022), 355-366.